Synthetic liquid-liquid phase separated RNA-protein biocondensates reveal a bi-phasic cytosol in *E.coli*

Authors: Naor Granik[1], Noa Katz[2], Sarah Goldberg[2], and Roee Amit[2,3*]

Affiliations:

[1] Department of Applied Mathematics, Technion - Israel Institute of Technology, Haifa 32000, Israel.

[2] Department of Biotechnology and Food Engineering, Technion - Israel Institute of Technology, Haifa 32000, Israel.

[3] The Russell Berrie Nanotechnology Institute, Technion - Israel Institute of Technology, Haifa 32000, Israel.

***** To whom correspondence should be addressed: roeeamit@technion.ac.il.

Abstract: Observations of liquid-liquid phase-separated compartments within living cells have generated important insights on intracellular processes in recent years. Here, we use PP7-coat protein and Qβ-coat protein together with multi-binding-site RNA scaffolds to generate synthetic phase-separated biocondensates within *E. coli* cells. Real-time tracking of entry and shedding of RNA-protein complexes into and out of the biocondensates reveals that the cytosol is divided into a dense liquid phase in the nucleoid-dominated region, and a dilute liquid phase in the polar regions. We provide evidence for this assertion using stationary phase cells, where emergence of non-polar biocondensate formation is consistent with a reduction in size of the dense-nucleoid phase. The bi-phasic hypothesis for the *E.coli* cytosol has implications for various transcriptional and translational processes, and could provide an alternative explanation for the Super-Poisson dynamics attributed to transcriptional bursts.

One Sentence Summary: Using synthetic liquid-liquid phase-separated biocondensates, we show that the *E.coli*'s cytosol is likely composed of a dense and dilute liquid phases.

Main text:

Liquid – liquid phase separation (LLPS), the process by which a homogeneous solution separates into molecularly dense and dilute liquid phases, has been connected to a wide range of natural cellular processes in virtually all forms of life (*1–5*). In cells, LLPS results in the formation of membrane-less compartments containing a high-concentration mix of biomolecules (e.g. proteins, RNA and proteins, etc.) Examples of such compartments include paraspeckles, stress granules, and nuclear speckles among others (*1*, *6*). Given the ubiquity of these compartments in cells, we hypothesized that it was possible to engineer a synthetic, orthogonal, and programmable phase separation system, and thereby provide an additional level of control over gene expression in synthetic systems (i.e. signal amplification and attenuation). As a proof of principle, we opted to trigger liquid-liquid phase separation using protein-RNA interactions in bacteria. The choice was based on the following observations: first, there have been multiple documented cases of LLPS triggered by long noncoding RNAs (lncRNAs) that are bound by various RNA binding proteins (RBPs) (*2*, *7*, *8*). These nucleoprotein complexes are evolutionary conserved and have been shown to play

an important regulatory role. Second, labelling RNA molecules using a fusion of the phage coat protein of MS2 or PP7 to a fluorescent protein by inserting a set of stem loops into the 5' or 3' end of the transcript has become commonplace in the last two decades (*9–14*). This approach, originally introduced by Singer and others (*9-11*), was devised for the purpose of probing the dynamics of transcription and other RNA-related processes, irrespective of cell-type. When co-expressed, the coat-protein-bound RNA cassettes yield bright puncta, which can be tracked in living cells. Given the similarities between the puncta signal attained from these cassettes and natural liquid-liquid phase separated puncta such as paraspeckles, we further hypothesized that these synthetic modular RNA scaffolds trigger liquid-liquid phase separation within different cell types, and that the observed puncta correspond to synthetic biocondensates.

To provide evidence for this hypothesis, we designed two synthetic long non-coding RNA (slncRNA) binding-site cassettes using our binding site resource (*15, 16*). The first slncRNA, Qβ-5x_ PP7-4x, consisted of five native Qβ and four native PP7 binding sites, in an interlaced manner. The second slncRNA, Qβ-10x, consisted of ten novel high-affinity (*17*) Qβ binding sites (Fig. 1A). The new slncRNA cassettes and the PP7-24x cassette (*18*) were each cloned downstream to a pT7 promoter on a single copy plasmid and transformed into BL21-DE3 *E. coli* cells, together with a plasmid encoding for either Qβ-mCherry or PP7-mCherry fusion proteins from an inducible promoter. Single cells expressing the cassettes and RBPs were imaged every 10 seconds for 60 minutes under constant conditions on an epi-fluorescent microscope. For all cassettes used in the experiment, the images revealed formation of various puncta at the majority of cell poles (Fig. 1B). Quantifying the fraction of cells that display at least one punctum reveals a dependence on the number of binding sites, in accordance with the multivalency model of LLPS formation (*19, 20*) (Fig. 1C). To provide further evidence that these puncta are phase-separated liquid droplets, we lysed cells expressing the Qβ-mCherry fusion protein only, and cells expressing both the fusion protein and the binding site cassette consisting of ten Qβ binding sites. We then measured the turbidity of the cell lysates. The results (Fig. 1D) show a 1.7-fold increase in turbidity (measured at OD600), a known signature of a liquid suspension containing phase separated droplets (*21, 22*). We further examined the cell lysates via flow cytometer and verified the existence of a second population characterized by denser particles that are mixed within a dilute liquid in the lysate containing the binding sites cassette (Fig. S1).

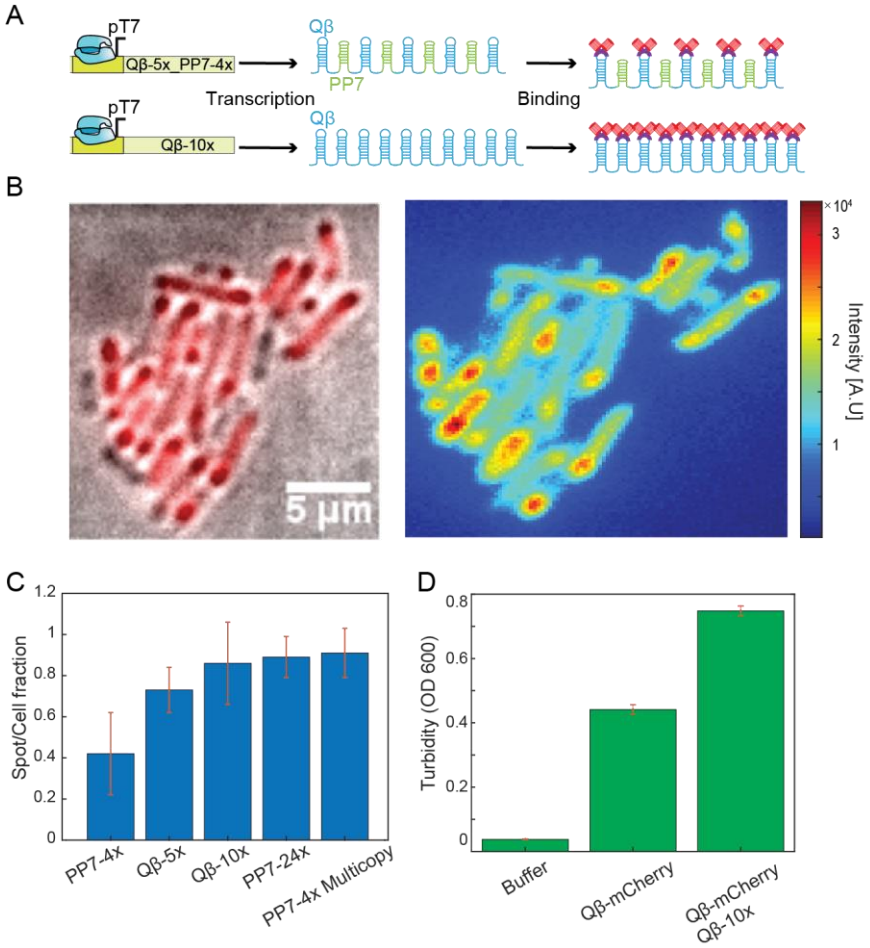

Figure. 1. Synthetic liquid-liquid phase separated droplets within bacterial cells. (A) Construct diagram depicting pT7 expression of the two new slncRNA cassettes used in this study, in the presence of Qβ-mCherry. (B) (left) Fluorescent image of cell expressing the Qβ-5x-PP7-4x slncRNA together with Qβ -mCherry. (right) Heatmap depiction of the image on left showing puncta within cells. (C) Cell fraction showing puncta as a function of cassette-type. Note, PP7-4x and Qβ-5x indicate the Qβ-5x-PP7-4x cassette expressed together with PP7-mCherry or Qβ-mCherry, respectively. Error bars indicate standard deviation (D) Turbidity (absorption) measurements of cell lysates that either contain the Qβ-5x-PP7-4x slncRNA (right) or not (middle).

Next, we analyzed the signal brightness of each punctum for every time point using a customized analysis algorithm (see Supplementary Methods and Fig. S2-S6). In Fig. 2A, we plot representative intensity vs time signals for the Qβ-5x-PP7-4x cassette together with Qβ-mCherry (denoted Qβ-5x), obtained from multiple puncta tracked in different fields of view on separate days (40 repetitions in total). The signals are either decreasing or increasing in overall intensity and dispersed within them are sharp variations in brightness, that are also either increasing or decreasing, which we termed "signal bursts". Next, we employed a statistical threshold which flagged these signal variation events whose amplitude was determined to not be part of the underlying signal noise (p-value<1e-3) (See Methods for definitions of bursts, algorithm details, and relevant numerical controls). These events were classified as either increasing signal bursts (green), decreasing signal bursts (red), and non-classified segments (blue) (Fig. 2A). In Fig. 2B we plot the distributions of amplitude (ΔI) for all three event types, obtained from ~300 puncta traces for the Qβ-5x data. The plots show the distributions of the three separated populations of non-classified, increasing, and decreasing signal bursts, with the number of positive and negative burst events being approximately equal. Moreover, a similarly symmetric burst distribution is recorded for the PP7-4x, Qβ-10x, and PP7-24x cassettes (Fig. S7).

A hallmark of LLPS (*3*, *22*) is the free exchange of molecules between the biocondensate droplet and the surrounding dilute phase. These exchange events are predicted to occur independently of one another at some rate that depends on the transient concentration of the molecules in the dilute phase (*20*). We examined whether our data supports this prediction, namely, whether positive and negative burst rates are independent. Specifically, we checked whether there was a bias for one type of burst or the other after a non-classified period that lasted more than 2.5 minutes (see Supplementary methods). The results (Fig. 2C) show that no such bias seems to exist, i.e., either a positive or negative burst seems to occur after non-classified events with equal probability for all four cassette types, consistent with the LLPS model. We then measured the amplitudes of the bursts for all four cassette-RBP pairings and found that both positive and negative amplitudes are proportional to the number of binding sites within the encoded cassette. (Fig. 2D). Together, these lines of data provide strong support that the bursts indeed correspond to insertion and shedding of slncRNA-RBP complexes into and from the denser droplet phase, respectively.

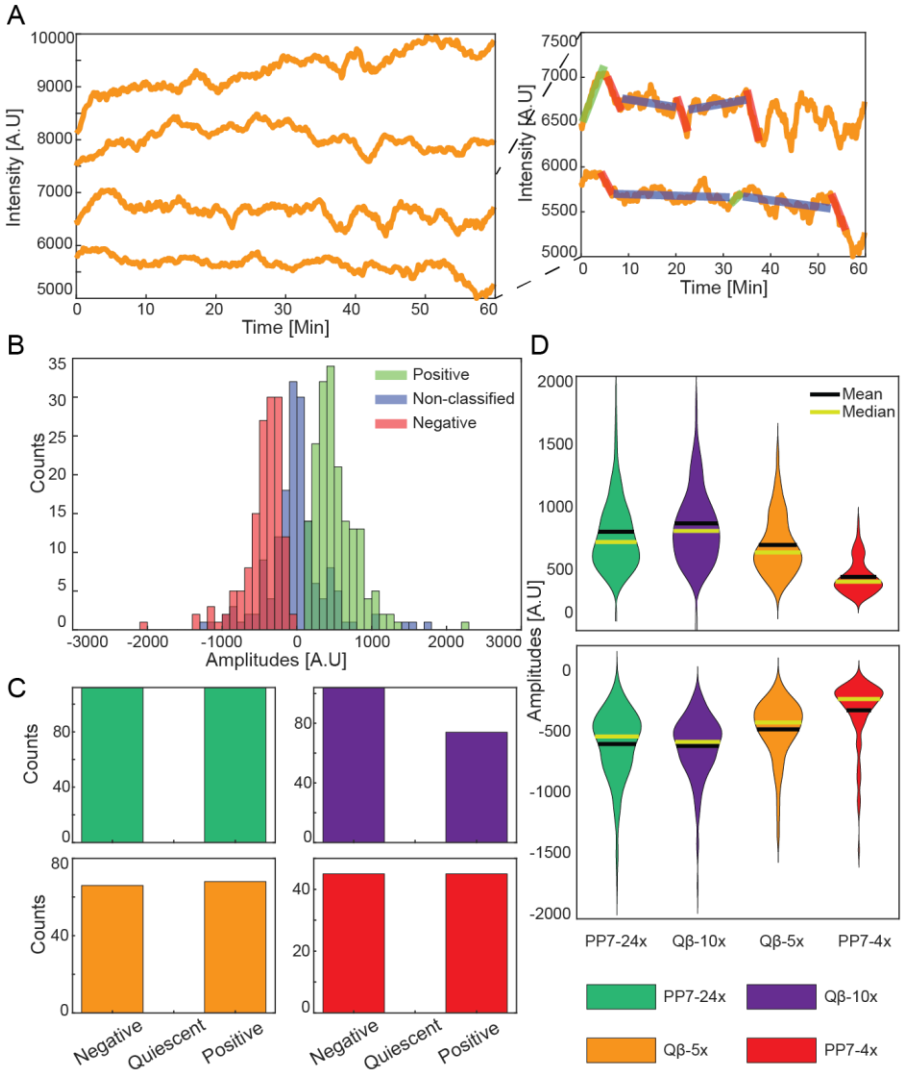

Figure. 2. Fluorescent puncta are characterized by insertion and shedding events of RNA-RBP complexes. (A) (left) Sample traces of puncta signal for the Qβ-5x cassette. (Right) Sample annotation of traces with positive bursts (green), negative bursts (red), and non-classified signal (blue), respectively. (B). Amplitude distribution for the different types of events, from 300 Qβ-5x traces. (C) Bar-graph showing the number of events for both negative and positive bursts immediately following a long (>2.5 min) non-classified event. From top-left, in clockwise direction: PP7-24x, Qβ-10x, PP7-4x, Qβ-5x. (D) Violin plots showing amplitude distribution as a function of cassette type for both positive (top) and negative (bottom) bursts.

In order to further characterize the shedding and insertion dynamics occurring between the biocondensate and the surrounding dilute phase, we estimated the number of slncRNA-RBP complexes that exist within the denser droplet phase. To do so, we fitted each shedding and insertion event amplitude distribution to a Poisson model which is justified by the uncorrelated occurrence of insertion and shedding events as a function of time (Fig. 2C). Fig. 3A-B present a sample fit for the PP7-4x burst amplitude distribution data, with three Poisson functions for $\lambda = 1$ (red), 2 (green), and 3 (black), corresponding to a mean of 1, 2, and 3 slncRNA-RBP complexes per burst, respectively. The fits show that while the $\lambda=3$ distribution provides the best fit to the data (corresponding to a mean of three slncRNAs per burst), the $\lambda=1$ distribution provides the best fit to the tail of the distribution, but fails at lower amplitude values. This may be due to our analysis threshold that treats many of these small amplitude events as unclassified. Higher values of λ provide a progressively worse fit. We repeated this analysis for the three additional cassette configurations and computed the estimated intensity per slncRNA-RBP complex (K_0) for each slncRNA-type (Fig. S8). Both the Poisson fits (Fig. 3C) and empirical distribution analysis (Fig. 2D) suggest that at least for the range of 4-10 binding sites, the number of sites in a cassette can be determined by the amplitude distribution at a resolution as low as a single binding site with a fluorescence signature that can be estimated to be~40-60 A.U. Using the single molecule intensity estimate obtained from the $\lambda=1$ approximation, we computed an estimate for the number of slncRNA-RBP complexes within each punctum, averaged over the duration of the trace. We then plotted the distribution of the average number of complexes per punctum, for each cassette-RBP pairing (Fig. 3D). The results show that for the Qβ-5x, Qβ-10x, and PP7-24x slncRNA cassettes puncta are estimated to contain ~10-30 slncRNA-RBP complexes, while the puncta for the PP7-4x cassette seem to be comprised of about half this number.

In the context of liquid-liquid phase-separation, such a difference between cassettes can occur if the dilute phase containing the PP7-4x molecules can tolerate a higher concentration of this slncRNA as compared with the other slncRNAs (and thus have a higher intensity). This is consistent with the multivalency hypothesis for LLPS (*19, 20*), which suggests that the volume fraction or concentration at which the LLPS transition occurs could depend strongly on the number of binding sites in the scaffold molecule. If so, and relying on the model developed by Klosin et. al.(*20*), this then implies that the rate of addition or shedding of a PP7-4x slncRNA-RBP complex into and from the droplet phase should be ~x2 faster as compared with the other complexes. To test this, we examined the time-interval between insertion events for all four slncRNA-RBP pairs. The time-interval distributions exhibited an exponential behavior (Fig. 3E), which is expected from a Markov-type process, as is apparently the case here. However, the average time-intervals between insertion events for each slncRNA-type (Fig. 3F) show that contrary to the multivalency model prediction, the mean time interval between bursts of signal increases for the PP7-4x cassette was ~ 2x slower as compared with the higher-valency configurations. To provide further support

for this anomalous observation, we measured directly the average level of the non-puncta background signal. The result shows a significantly lower signal intensity for the PP7-4x slncRNA background (Fig. 3G), which is consistent with the longer mean interval between events observe for this cassette.

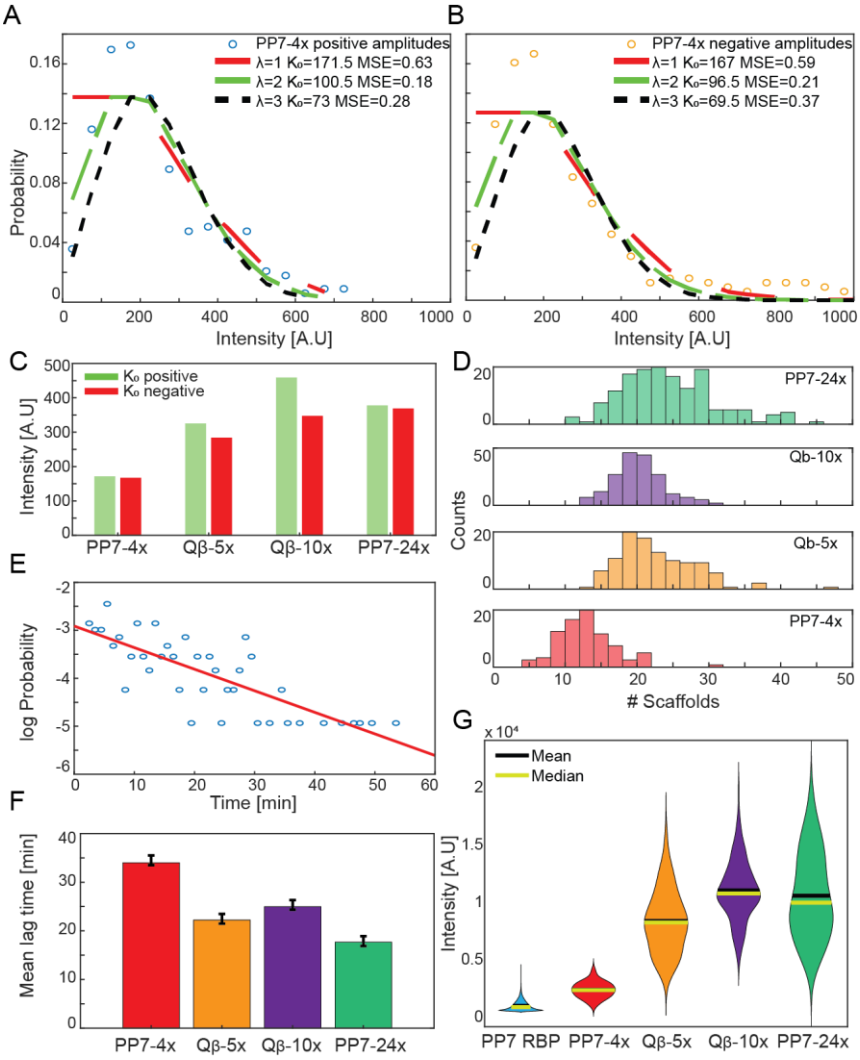

Figure. 3. Puncta analysis suggests a biphasic cytosol in *E. coli*. (A-B) Poisson functions fits for the amplitude distribution of insertion assuming 1, 2, or 3 mean events (A) and shedding (B) events. (C) Extracted fluorescence signal for a single slncRNA-RBP complex, assuming a Poisson distribution with λ=1. (D) Distribution corresponding to the number of slncRNAs per puncta, assuming the value of K_0 shown in panel (C). (E) Lag-time distribution between insertion events for Qβ-5x r-square of fit is 0.63.(F) Bar plot showing extracted mean lag times for all four cassette-RBP pairings. Error bars indicate 95% confidence intervals (G) Violin plot showing mean background levels from cells expressing the PP7-mCherry fusion protein only (light blue), and cells expressing slncRNAs together with the fitting fusion protein (red, orange, purple and green corresponding to PP7-4x, Qβ-5x, Qβ-10x and PP7-24x)

In order to accommodate these contradictory findings within a broader LLPS context, we hypothesized that the *E. coli* cytosol consists of a dense molecular phase in the central portion of the cell consistent with the location of the nucleoid (*23*), and a dilute molecular phase in the polar regions. As a result, slncRNAs cannot phase separate and form biocondensates within the dense-nucleoid phase. In contrast, the polar regions of the *E. coli* cell are sufficiently dilute to facilitate formation of biocondensates, as observed in our experiments (see Fig. 4A for model schematic and Supplementary text). In this scenario, the dense cytosolic nucleoid phase serves as a reservoir of slncRNA molecules, which when released into the polar regions phase separate into the biocondensate droplets. For the case of PP7-4x, we assume that reduced stability of the slncRNA scaffold within the dense nucleoid-region reservoir as compared with the other slncRNAs may lead to a reduced background signal, which in turn leads to a lower mean rate of entry into the droplet and to fewer molecules within the droplet. A possible reason for this instability is misfolding of the scaffold due to the spatial positioning of the occupied binding sites, increasing its vulnerability to degradation. To provide support for the biphasic hypothesis of the bacterial cell, we carried out two additional experiments. In the first, we expressed the PP7-4x on a multicopy plasmid. The purpose of this experiment was to increase the background levels of the cassette, which according to our biphasic model and data from the other slncRNAs is predicted to lead to an increase in the number of cassettes within the biocondensate droplets. As Fig. 4B shows, we indeed witnessed an increase in both the background signal, and in the number of estimated scaffolds within the puncta (Fig. 4B), to levels similar to the ones observed with the other slncRNAs. In the second, we grew the cells in starvation conditions for several hours, triggering a transition to stationary phase. In stationary phase the nucleoid is known to condense (*24–26*), thus increasing the amount of cellular volume which is likely to be molecularly dilute. This, in turn, generates a much larger accessible cellular volume for droplet formation, which should lead to different presentation of the phase-separation phenomena as compared with exponentially growing cells. In Fig. 4C, we show images of bacteria displaying ‘bridging’ (the formation of a high intensity streak between the spots) of puncta (left), whereby biocondensates seem to fill out the available dilute volume, and the emergence of a third puncta at the center of the cell (center). Both behaviors are substantially different than the puncta appearing under normal conditions (right). Such behavior was observed in >40% of the fluorescent cells and was not detected in non-stationary growth conditions.

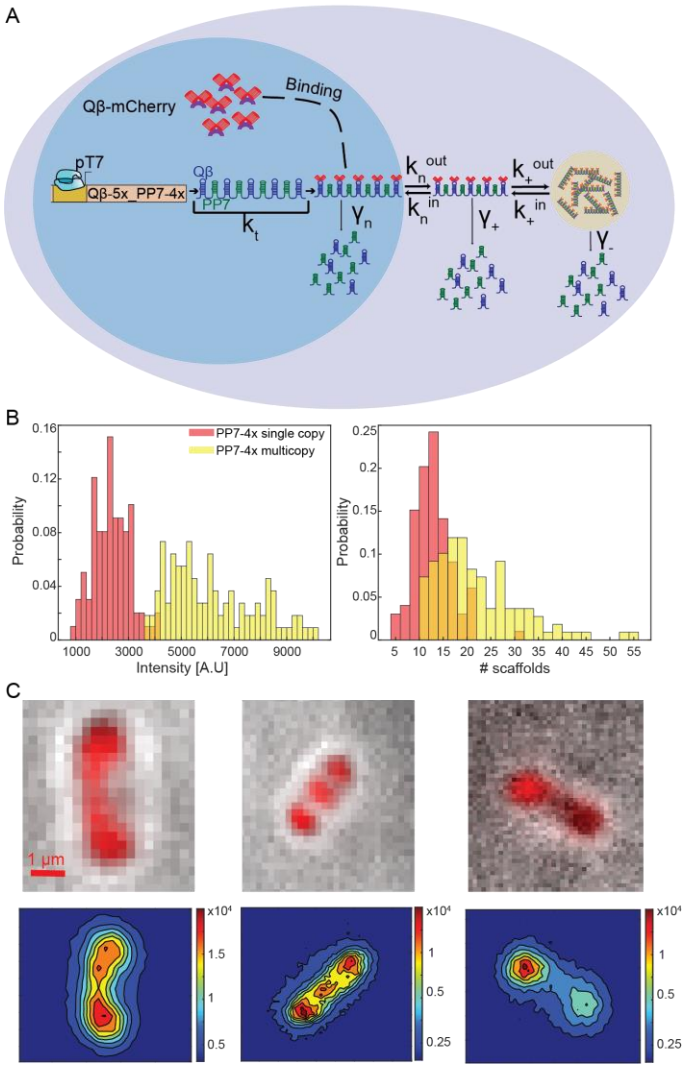

Figure. 4. Verification of biphasic cytosol hypothesis. (A) Model showing the effects of the biphasic hypothesis on insertion and shedding of a slncRNA. Parameters: k_t and γ_n are the slncRNA transcriptional and degradation rates, $k_n^{in/out}$ correspond to the rates by which the slncRNA-RBP complexes leave/re-enter the nucleoid phase, and , $k_+^{out/in}$ correspond to the insertion/shedding rates of the slncRNA-RBP complexes from the dilute to the droplet phase. The biphasic model is an extension of the simple rate-equation gene expression model and leads to a Super-Poisson distribution of RNA for any RNA species (see SI). (B) (left) Background fluorescence signal for the PP7-4x slncRNA expressed from a multi-copy plasmid (yellow) and single-copy plasmid (red). (right) Distribution of the number of slncRNA-RBP complexes within the puncta for each case. (C) (left and middle) Typical images of fluorescent bacteria in stationary phase, which are very different than the 2-puncta image obtained for exponentially growing cells (right). A close examination shows "bridging" or spreading of puncta (bottom-left), and emergence of an additional punctum in the middle of the cell (bottom-middle).

In this study, we used analysis of multiple types of slncRNA-RBP phase-separated droplets to propose a bi-phasic model for the *E. coli* cytosol. In our model the cytosol is composed of dense and dilute liquid phases. The dense phase is mostly associated with the nucleoid, while the dilute phase occupies the non-nucleoid regions of the cell. The immediate consequence of this model is that synthetic RNA-scaffolded phase-separated molecular biocondensates can only form in the dilute phase, which in exponentially growing cells correspond to the polar regions. Thus, since migration of RNA and assembly into localized condensates in the polar regions is a direct consequence of this model of liquid phase separation, RNA that is found in the poles is not likely to require an active mode of localization as for membrane or nucleoid targeting mRNAs (*27*). Moreover, a cell model with dense and dilute cytosolic liquid phases leads to an important consequence for gene-expression noise. Previous studies using various approaches have shown that mRNA of most genes exhibit a Super-Poisson distribution profile, which has been attributed to transcriptional bursting resulting from a promoter switching mechanism (*28–30*). By contrast, in the biphasic-model a super-Poisson distribution for gene expression emerges as a mechanism-independent and parameter-free prediction (see Fig. 4A and Supplementary Model). Therefore, this model corresponds to an Occam's razor explanation for the super-Poisson distributions (*12*, *14*, *29*, *31*) and if proven to be true by additional experimental studies is likely to have many implications for bacterial gene expression and RNA-related observations.

Supplementary Materials:

Materials and Methods

Supplementary text

Figures S1-S8

References (*31–36*)

References and Notes:

1. S. F. Banani, H. O. Lee, A. A. Hyman, M. K. Rosen, Biomolecular condensates: organizers of cellular biochemistry. *Nat Rev Mol Cell Biol*. **18**, 285–298 (2017).

2. M. Polymenidou, The RNA face of phase separation. *Science*. **360**, 859–860 (2018).

3. A. A. Hyman, C. A. Weber, F. Jülicher, Liquid-Liquid Phase Separation in Biology. *Annual Review of Cell and Developmental Biology*. **30**, 39–58 (2014).

4. E. M. Langdon, A. S. Gladfelter, A New Lens for RNA Localization: Liquid-Liquid Phase Separation. *Annual Review of Microbiology*. **72**, 255–271 (2018).

5. S. Boeynaems, S. Alberti, N. L. Fawzi, T. Mittag, M. Polymenidou, F. Rousseau, J. Schymkowitz, J. Shorter, B. Wolozin, L. Van Den Bosch, P. Tompa, M. Fuxreiter, Protein Phase Separation: A New Phase in Cell Biology. *Trends Cell Biol*. **28**, 420–435 (2018).

6. Y. S. Mao, B. Zhang, D. L. Spector, Biogenesis and function of nuclear bodies. *Trends Genet.* **27**, 295–306 (2011).

7. C. S. Bond, A. H. Fox, Paraspeckles: nuclear bodies built on long noncoding RNA. *J Cell Biol*. **186**, 637–644 (2009).

8. C. M. Clemson, J. N. Hutchinson, S. A. Sara, A. W. Ensminger, A. H. Fox, A. Chess, J. B. Lawrence, An architectural role for a nuclear noncoding RNA: NEAT1 RNA is essential for the structure of paraspeckles. *Mol. Cell*. **33**, 717–726 (2009).

9. E. Bertrand, P. Chartrand, M. Schaefer, S. M. Shenoy, R. H. Singer, R. M. Long, Localization of ASH1 mRNA particles in living yeast. *Molecular cell*. **2**, 437–445 (1998).

10. E. Tutucci, M. Vera, J. Biswas, J. Garcia, R. Parker, R. H. Singer, An improved MS2 system for accurate reporting of the mRNA life cycle. *Nature Methods*. **15**, 81–89 (2018).

11. D. R. Larson, R. H. Singer, D. Zenklusen, A Single Molecule View of Gene Expression. *Trends Cell Biol*. **19**, 630–637 (2009).

12. D. Jones, J. Elf, Bursting onto the scene? Exploring stochastic mRNA production in bacteria. *Current Opinion in Microbiology*. **45**, 124–130 (2018).

13. D. Fusco, N. Accornero, B. Lavoie, S. M. Shenoy, J.-M. Blanchard, R. H. Singer, E. Bertrand, Single mRNA molecules demonstrate probabilistic movement in living mammalian cells. *Current Biology*. **13**, 161–167 (2003).

14. I. Golding, J. Paulsson, S. M. Zawilski, E. C. Cox, Real-Time Kinetics of Gene Activity in Individual Bacteria. *Cell*. **123**, 1025–1036 (2005).

15. N. Katz, R. Cohen, O. Solomon, B. Kaufmann, O. Atar, Z. Yakhini, S. Goldberg, R. Amit, An in Vivo Binding Assay for RNA-Binding Proteins Based on Repression of a Reporter Gene. *ACS Synth. Biol.* **7**, 2765–2774 (2018).

16. N. Katz, R. Cohen, O. Solomon, B. Kaufmann, O. Atar, Z. Yakhini, S. Goldberg, R. Amit, Synthetic 5′ UTRs Can Either Up- or Downregulate Expression upon RNA-Binding Protein Binding. *Cell Systems*. **9**, 93-106.e8 (2019).

17. N. Katz, E. Tripto, S. Goldberg, O. Atar, Z. Yakhini, Y. Orenstein, R. Amit, Overcoming the design, build, test (DBT) bottleneck for synthesis of nonrepetitive protein-RNA binding cassettes for RNA applications. *bioRxiv*, in press, doi:10.1101/2019.12.24.886168.

18. S. Hocine, P. Raymond, D. Zenklusen, J. A. Chao, R. H. Singer, Single-molecule analysis of gene expression using two-color RNA labeling in live yeast. *Nature Methods*. **10**, 119–121 (2013).

19. P. Li, S. Banjade, H.-C. Cheng, S. Kim, B. Chen, L. Guo, M. Llaguno, J. V. Hollingsworth, D. S. King, S. F. Banani, P. S. Russo, Q.-X. Jiang, B. T. Nixon, M. K. Rosen, Phase transitions in the assembly of multivalent signalling proteins. *Nature*. **483**, 336–340 (2012).

20. A. Klosin, F. Oltsch, T. Harmon, A. Honigmann, F. Jülicher, A. A. Hyman, C. Zechner, Phase separation provides a mechanism to reduce noise in cells. *Science*. **367**, 464–468 (2020).

21. Z. Wang, G. Zhang, H. Zhang, Protocol for analyzing protein liquid–liquid phase separation. *Biophys Rep*. **5**, 1–9 (2019).

22. Z. Feng, X. Chen, X. Wu, M. Zhang, Formation of biological condensates via phase separation: Characteristics, analytical methods, and physiological implications. *J Biol Chem*. **294**, 14823–14835 (2019).

23. J. K. Fisher, A. Bourniquel, G. Witz, B. Weiner, M. Prentiss, N. Kleckner, Four-Dimensional Imaging of E. coli Nucleoid Organization and Dynamics in Living Cells. *Cell*. **153**, 882–895 (2013).

24. J. Kim, S. H. Yoshimura, K. Hizume, R. L. Ohniwa, A. Ishihama, K. Takeyasu, Fundamental structural units of the Escherichia coli nucleoid revealed by atomic force microscopy. *Nucleic Acids Res*. **32**, 1982–1992 (2004).

25. S. G. Wolf, D. Frenkiel, T. Arad, S. E. Finkel, R. Kolter, A. Minsky, DNA protection by stress-induced biocrystallization. *Nature*. **400**, 83–85 (1999).

26. R. Janissen, M. M. A. Arens, N. N. Vtyurina, Z. Rivai, N. D. Sunday, B. Eslami-Mossallam, A. A. Gritsenko, L. Laan, D. de Ridder, I. Artsimovitch, N. H. Dekker, E. A. Abbondanzieri, A. S. Meyer, Global DNA Compaction in Stationary-Phase Bacteria Does Not Affect Transcription. *Cell*. **174**, 1188-1199.e14 (2018).

27. S. Kannaiah, J. Livny, O. Amster-Choder, Spatiotemporal Organization of the E. coli Transcriptome: Translation Independence and Engagement in Regulation. *Molecular Cell*. **76**, 574-589.e7 (2019).

28. T. Lionnet, R. H. Singer, Transcription goes digital. *EMBO Rep*. **13**, 313–321 (2012).

29. J. Paulsson, Models of stochastic gene expression. *Physics of Life Reviews*. **2**, 157–175 (2005).

30. L. So, A. Ghosh, C. Zong, L. A. Sepúlveda, R. Segev, I. Golding, General properties of transcriptional time series in Escherichia coli. *Nature Genetics*. **43**, 554–560 (2011).

31. A. Sanchez, H. G. Garcia, D. Jones, R. Phillips, J. Kondev, Effect of Promoter Architecture on the Cell-to-Cell Variability in Gene Expression. *PLoS Computational Biology*. **7**, e1001100 (2011).

32. G. Medina, K. Juárez, B. Valderrama, G. Soberón-Chávez, Mechanism of Pseudomonas aeruginosa RhlR Transcriptional Regulation of the rhlAB Promoter. *Journal of Bacteriology*. **185**, 5976–5983 (2003).

33. C. A. Schneider, W. S. Rasband, K. W. Eliceiri, NIH Image to ImageJ: 25 years of image analysis. *Nature Methods*. **9**, 671–675 (2012).

34. J. Schindelin, I. Arganda-Carreras, E. Frise, V. Kaynig, M. Longair, T. Pietzsch, S. Preibisch, C. Rueden, S. Saalfeld, B. Schmid, J.-Y. Tinevez, D. J. White, V. Hartenstein, K. Eliceiri, P. Tomancak, A. Cardona, Fiji: an open-source platform for biological-image analysis. *Nature Methods*. **9**, 676–682 (2012).

35. I. F. Sbalzarini, P. Koumoutsakos, Feature point tracking and trajectory analysis for video imaging in cell biology. *J. Struct. Biol.* **151**, 182–195 (2005).

36. N. Otsu, A Threshold Selection Method from Gray-Level Histograms. *IEEE Transactions on Systems, Man, and Cybernetics*. **9**, 62–66 (1979).

Acknowledgments: The authors would like to acknowledge the Technion's LS&E staff (Tal Katz-Ezov and Anastasia Diviatis) for help with sequencing and some imaging experiments. In addition the authors would like to thank professor Yoav Schectman from the Department of Biomedical Engineering in the Technion for help with image and signal analysis.

Funding: This project received funding from the I-CORE Program of the Planning and Budgeting Committee and the Israel Science Foundation (Grant No. 152/11); Marie Curie Reintegration Grant No. PCIG11-GA-2012-321675; and from the European Union's Horizon 2020 Research and Innovation Programme under grant agreement 664918 (MRG-Grammar) and 851065 (CARBP).

Author contributions: NG designed and carried out the microscopy experiments and analysis for all data. NK designed and synthesized the PP7-4x-Qβ-5x and Qβ-10x cassettes. SG assisted and guided the experiments and image analysis. RA supervised the study. NG and RA wrote the manuscript.

Competing interests: The authors declare no competing interests.

Data and materials availability: All datasets and original code used in this paper are available from: https://github.com/naorgk/slncRNA_Analysis. All bacterial plasmids constructed for this work are available upon request.